frontiers | Frontiers in Materials

TYPE Original Research
PUBLISHED 29 January 2024
DOI 10.3389/fmats.2024.1328347

OPEN ACCESS

EDITED BY
Qingzhen Yang,
Xi'an Jiaotong University, China

REVIEWED BY
Muhammad Yasir Khalid,
Khalifa University, United Arab Emirates
Zia Ullah Arif,
University of Southampton, United Kingdom

*CORRESPONDENCE
Hushein R,
husheinece@gmail.com

RECEIVED 13 November 2023
ACCEPTED 11 January 2024
PUBLISHED 29 January 2024

CITATION
R H, Shajahan MI, Čep R, Salunkhe S, Murali AP, Sharad G, Mohamed Abdelmoneam Hussein H and Abouel Nasr E (2024), Electrical conductivity analysis of extrusion-based 3D-printed graphene. *Front. Mater.* 11:1328347. doi: 10.3389/fmats.2024.1328347

Electrical conductivity analysis of extrusion-based 3D-printed graphene

Hushein R[1]*, Mohamed Iqbal Shajahan[2], Robert Čep[3], Sachin Salunkhe[4,5], Arun Prasad Murali[2], Gawade Sharad[6], Hussein Mohamed Abdelmoneam Hussein[7] and Emad Abouel Nasr[8]

[1]Department of Electronics Engineering, Vel Tech Rangarajan Dr. Sagunthala R&D Institute of Science and Technology, Chennai, India, [2]Department of Mechanical Engineering, Vel Tech Rangarajan Dr. Sagunthala R&D Institute of Science and Technology, Chennai, India, [3]Department of Machining, Assembly and Engineering Metrology, Faculty of Mechanical Engineering, VSB Technical University of Ostrava, Ostrava, Czechia, [4]Department of Biosciences, Saveetha School of Engineering, Saveetha Institute of Medical and Technical Sciences, Chennai, India, [5]Mechanical Engineering Department, Faculty of Engineering, Gazi University, Ankara, Turkiye, [6]Sharadchandra Pawar, College of Engineering and Technology, Baramati, India, [7]Mechanical Engineering, Faculty of Engineering, Helwan University, Cairo, Egypt, [8]Department of Industrial Engineering, College of Engineering, King Saud University, Riyadh, Saudi Arabia

Nowadays, research has shown the emergence of the 3D printing method for printing a functionalized component. Graphene nanomaterial has an enormous conducting property that can compete with conducting materials like copper and silicon. This paper describes the electrical conductivity investigation of 3D-printed graphene nanomaterial in extrusion-based 3D printing methods. In extrusion, two different approaches of the 3D printing method were used to print the graphene-based structure: the fused deposition modeling (FDM) method and the direct ink writing (DIW) method. Both printing methods follow the two printing processes and select material forms. Selection of testing was made to analyze the characterization variations in the printed material, such as XRD, TGA, viscosity, Raman shift, and Scanning Electron Microscopy analyses, which shows the changes of effect in the conductivity due to various parameter differences in both the printing methods. A four-point probe technique was used to analyze the electrical conductivity of the two different methods. These analysis results prove that the characterization variations differ in the FDM and DIW printed models.

KEYWORDS

3D printing of conductive materials, graphene nanomaterial, fused deposition modeling, direct ink writing, electrical conductivity

Abbreviations: Three dimension, 3D; direct ink writing, DIW; fused deposition modeling, FDM; silicon, Si; multi-walled carbon nanotube, MWCNT; poly-lactic acid, PLA; polyvinyl alcohol, PVA; X-ray diffraction, XRD; thermogravimetric analysis, TGA; structural equation modeling, Scanning Electron Microscopy.

1 Introduction

In the current scenario, manufacturing industries have experienced rapid growth. Materials and manufacturing methods have been expanding at two different levels. Materials are considered the major source, providing more ways to manufacture different types of products. However, in traditional manufacturing, it is more difficult to produce the same product with different forms of materials and to manufacture a complex shape (Ngo et al., 2018). However, additive manufacturing is unique, frequently allowing different materials like plastics, powders, resins, and metal to print a single structure in a complex form. Additive manufacturing methods involve adding a material layer by layer based on the designed 3D structure to form the physical structure and make a product in the physical structure (Bikas et al., 2016).

Moreover, compared with traditional manufacturing methods, additive manufacturing methods can provide more flexibility in the design and choice of multiple forms of materials, which can enable the printing of lightweight and complex designed structures (Arif et al., 2023; Arif et al., 2022; Khalid et al., 2023a). Graphene is a 2D single-crystal carbon atom; the structure has a thick sp2 bonding. It is a two-dimensional honeycomb structure with unique properties. Compared with silicon (Si), graphene has a very high (100 times) electron mobility and conducts heat two times better than diamond. Compared with other characteristics, shown in Table 1, graphene has the most important unique properties: it is a zero-overlapping semi-metal material with high electrical conductivity (Gnanasekaran et al., 2017; Arif et al., 2023; Khalid et al., 2023b). The characteristics of graphene's electronic properties are elucidated by a two-dimensional counterpart of the Dirac equation, as opposed to the Schrödinger equation, which governs the behavior of spin-1/2 particles. This distinctive attribute enables electrons to traverse graphene's honeycomb lattice, effectively shedding their mass and giving rise to quasi-particles capable of transporting and transmitting an electrical charge (Tarelho et al., 2018; Mansour et al., 2019). Agudosi et al. (2020) executed the experiments to evaluate the multiple ways of producing single-layer graphene and different graphene-based composites. The formulation of both graphene elements leads to energy storage applications. Zhang et al. (2016) showed the modified two-step *in situ* methods to improve the conductivity of graphene with the addition of PLA, and the result expressed it having good mechanical strength. The above two studies show that graphene has better conductivity and mechanical strength than any other material under FDM printing methods. Buzz (Wincheski et al., 2019) described the direct printing of RGO strain sensors to have the capability of coupled flexibility, conductivity, and a smooth solution process. This result showed that RGO strain sensors are capable of robust and accurate measuring elements. Mattevi (2021) described the rheological behavior of functional-based ink composition, which is prepared for the direct ink writing (DIW) printing process of energy materials. This study explained the detailed characterization of ink rheological properties of different energy materials and suggested increasing the printing speed to increase the number of products. Adaris et al. (2020) fabricated a 3D electrochemical biosensor using FDM printing for environmental and biomedical applications. These results show the biocompatibility of the 3D-printed model and its ability to produce the output model without the need for electron mediators. Solís Pinargote et al. (2020) reviewed the various examples of graphene with several additive manufacturing technologies and summarized the principles and applications.

TABLE 1 Graphene comparison with other competing materials.

Property	Graphene	Competing materials	
Strength	130 GPa	Steel	0.41 GPa
Thermal conductivity	~5000 W/m.k	Copper	400 W/m.k
Electrical conductivity	$\sim 10 \times 10^7$ S/m	Copper	58.5×10^6 S/m
Weight	0.002 g/m^2	Paper	~0.75 g/m2

Moreover, these studies focused on the development of DIW with graphene nanomaterial. Ivanov et al. (2019) explored the unique properties of graphene, like its thermal and electrical properties. The morphological properties of graphene have been studied from the different content ratios with multi-walled carbon nanotubes (MWCNTs). These results identified the correlation between low-cost industrial graphene (6 wt%) and MWCNTs and found the synergetic effect of several mono-level combinations with bi-filler level mixtures. The output results show an increase in the electrical conductivity of graphene with PLA more than MWCNTs, and also, it clearly indicates the relationship between both the thermal and electrical properties of graphene/PLA composites1. Finally, the analysis has found that these composites have outstanding electrical and thermal properties for various levels of applications. The direct ink writing (DIW) printing method is derived from the extrusion level-based method, which describes computer-controlled fabrication methods (Khalid et al., 2023a; Noroozi et al., 2023).

A primary feature of this method is having boundless freedom in material selection, especially for conductive inks. It belongs to the category of soft lithography and is one of the most highly reliable methods for producing micro-patterns with a lightweight design (Lei et al., 2012; Sabet and Soleimani, 2019; Tsang et al., 2020; Guo et al., 2021). The additive manufacturing (AM) process has different methods for 3D printing products compared with other methods. Fused deposition modeling (FDM) has the unique features of more advantages, including the easy process of printing, cost, and time effectiveness (Jing et al., 2020; Larraza et al., 2021). It is also considered more affordable than other methods. Nowadays, many researchers are moving toward FDM, which is revolutionizing the manufacturing industries to fulfill their demands based on technology development (Rajpurohit and Dave, 2019; Kristiawan et al., 2021).

1.1 Contribution

The main aim and novelty of this present work is to discuss the analysis of the electrical conductivity of graphene for two different 3D printing methods, namely, FDM and DIW, of graphene nanomaterial, as mentioned in the proposed model diagram (Figure 1). First, the procedure for the preparation of materials for the two different printing methods is presented. Second, we

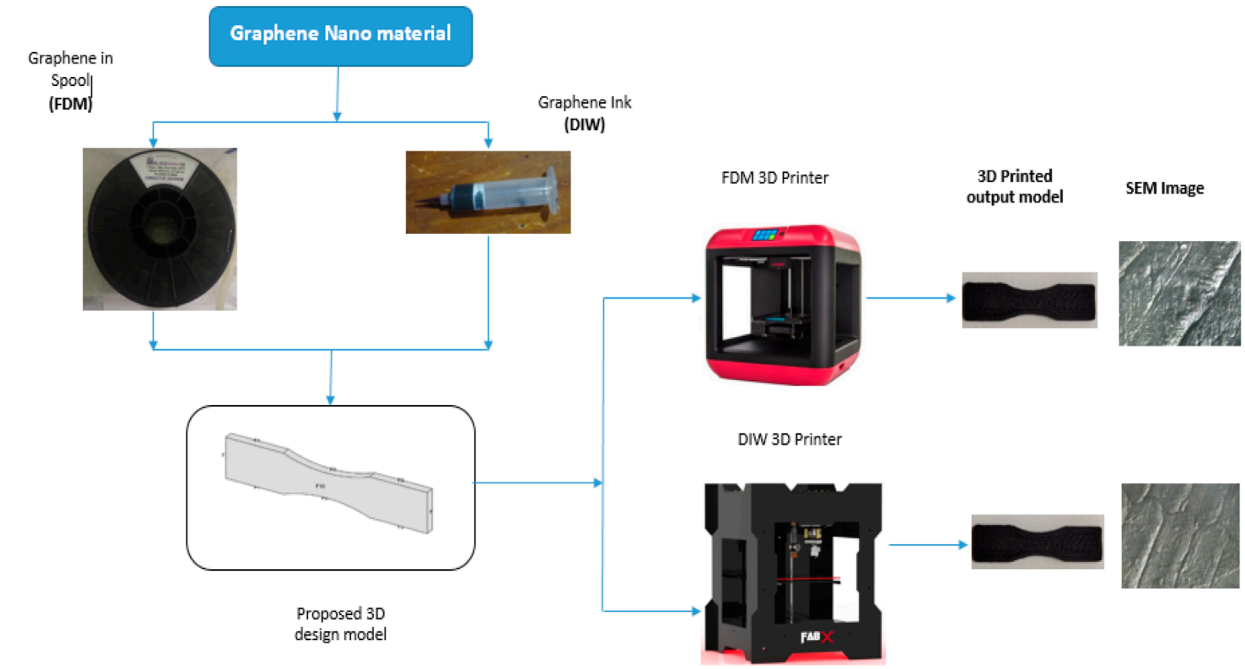

FIGURE 1
Proposed methodology for printing a 3D-printed model using DIW and FDM methods.

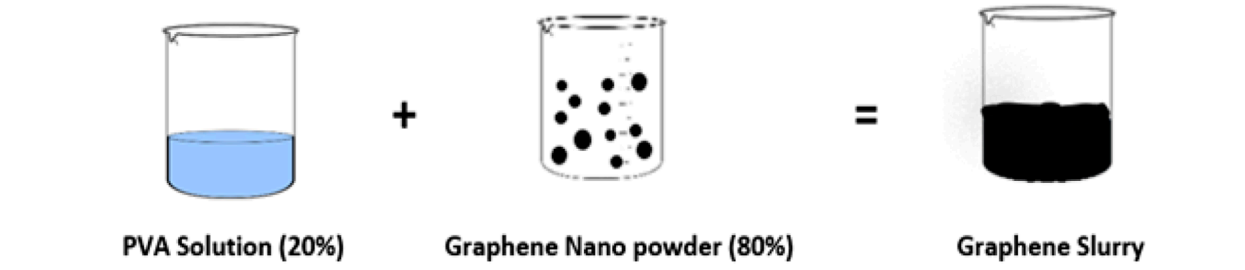

FIGURE 2
Graphene slurry preparation.

discussed detailed information about the effects of changes in each testing method, following XRD, TGA, viscosity, and Raman shift analyses. The XRD technique was used to define the structure and bonding between the carbon atoms, the TGA analysis examined the decomposition analysis, and viscosity showed the feasibility of the printing material on the surface and Raman shift analysis of the band structure and surface layer. All these characterization changes show how the conductivity varies for the two printing methods.

2 Experimental procedure

2.1 Material preparation

This paper proposes two different 3D printing methods to print graphene nanomaterial: the direct ink writing (DIW) method and the fused deposition modeling (FDM) method. Both printing methods had the same variety of approaches for preparing the graphene nanomaterial for use in the printing method (Wei et al., 2015; Student-member and Wolterink, 2020). The PVA solution was prepared by forming 15% of polyvinyl alcohol (PVA) and 85% of DI water (Figure 2). From those, 10 g of the PVA solution was taken for preparation of the slurry. Once the PVA solution was prepared, the graphene slurry was prepared to form 20% and 80%, respectively, with the graphene nanomaterial and PVA solution (Papageorgiou et al., 2017; Sun et al., 2020; Daniel and Liu, 2021).

2.2 Printing method

2.2.1 DIW

DIW is a modest, protean approach appropriate for many kinds of materials available in the market. Most importantly, it is the easiest method to fabricate 3D prototypes (Yang et al., 2020; Hou et al.,

2021). Graphene powder was obtained from Black Magic 3D. The prepared graphene slurry depicted in Figure 2 was filled in a tube and fit with a 3D printer. Based on the 3D-designed model, viscosity and pressure were the input parameters, and the material was poured into the desired point (Tricot et al., 2018; Solís Pinargote et al., 2020). The continuous point makes and completes one layer, and the required 3D-designed model is developed layer by layer. The rheology behavior and surface morphology of the printed material are important factors that make it different from other 3D printing methods (Jing et al., 2020; Mogan et al., 2021). The main concept of the technique is close to the FDM printing method.

After the completion of the experimental process, the designed model is printed with the anticipated results. The printed model accurately reflects the intended dimensions. Figure 3 illustrates the processing and the printed model.

2.2.2 FDM

In FDM processing, the 3D printer utilized is from FlashForge Corp. The graphene material spool, obtained from Black Magic 3D, is securely placed into the 3D printer. The printing parameters dictate that the material is extruded at approximately 180°C, using a 0.4-mm nozzle to achieve the desired design model (Liu et al., 2019; Guo et al., 2021). To regulate the printing process (Liu et al., 2018), all the relevant process parameters are inputted into FlashPrint with Slicer software. Throughout the printing procedure, the printer's temperature is carefully set to 50°C for the build platform and 210°C for the extrusion. The printing parameters of the above two printing methods are shown in Table 2. Figure 4 depicts the processing and the printed model.

FIGURE 3
Graphene slurry preparation and printed model.

TABLE 2 Printing parameters.

3D printing parameter	FDM	DIW
Build plate temperature	80 [°C]	80 [°C]
Printing temperature	230 [°C]	230 [°C]
Printing speed	25 [mm/s]	25 [mm/s]
Layer height	0.1 mm	0.1 mm
Nozzle diameter	0.4 mm	0.4 mm
Infill	30%	30%

3 Characterization techniques

In this proposed research work, graphene is considered the raw material. The aim is to understand the nature and structural behavior of the material. Each characterization method in this analysis determines some specific behavior of the 3D-printed graphene (Jo et al., 2012; Foster et al., 2017; Sabet and Soleimani, 2019). The XRD technique is used to analyze the crystal structure of the graphene. It represents the rise in the interlayer space, and the distance between the carbon atoms available in the planes of graphene increases from the peak value (Feng et al., 2019). Figure 5A shows the collected XRD pattern of the printed graphene sample. For ease of representation, the *Y*-axis of the graph is linear from 0° to 80° CPS, and the *X*-axis of the graph has mentioned 2Θ value within the ranges from 0° to 60°. Indexing and lattice parameters were calculated using an analytical technique for indexing. Graphene is a highly crystalline material having a hexagonal lattice with P63/MMC space group symmetry. The XRD analysis shows that a strong characteristic peak is observed at 2Θ = 17.63° for DIW and 2Θ = 31.63° for FDM, corresponding to d = 3.34410 Å. The characteristic peak of graphite by the 002 plane shows a sharp and very high peak, indicating a highly crystalline structure and its orientation.

Moreover, it shows the disruption of planer stacking but still has the presence of some residual planer sequence in exfoliated forms. Significant peaks of 004 and 006 planes for FDM are observed at 2Θ = 21.74°, 37.55°, and 44.71°, respectively, and for DIW, they are observed at 19.12° and 26.90°, respectively. The d-spacing of graphene experiences an increase as a result of the strong interaction between PLA and PVA with graphene, respectively.

Conversely, the d-spacing for graphene undergoes a decrease, which can be attributed to the successful reduction of graphene oxide. Notably, no crystalline peaks were observed in the composition of graphene. However, unlike FDM, DIW exhibits a significantly lower number of peaks. Consequently, the interlayer interaction between graphene and PVA is considerably diminished. Furthermore, this overall reaction is attributed to the formation of an irregular structure caused by the dilution effect of the polymer matrix, and the highly exfoliated graphene sheets are dispersed within the PMMA matrix.

The decomposition analysis of the graphene nanomaterial with PLA was examined using thermogravimetric analysis (Ku et al., 2020) (TGA) (Figure 5B). It was conducted utilizing a NETZSCH STA 2500 Regulus system. The 3D-printed samples were focused on a steady temperature increase of 10°C/min, over 25°C–800°C. Graphene exhibited a major loss between 280°C and 370°C and 345°C and 505°C for FDM and DIW, respectively. The number of variations in the heat energy collapses in the structure of the hexagonal carbon framework due to breakage between the sp2 hybridized carbon atoms with covalent bonds. DIW exhibited a rapid detachment in the bond between the carbon atom, while

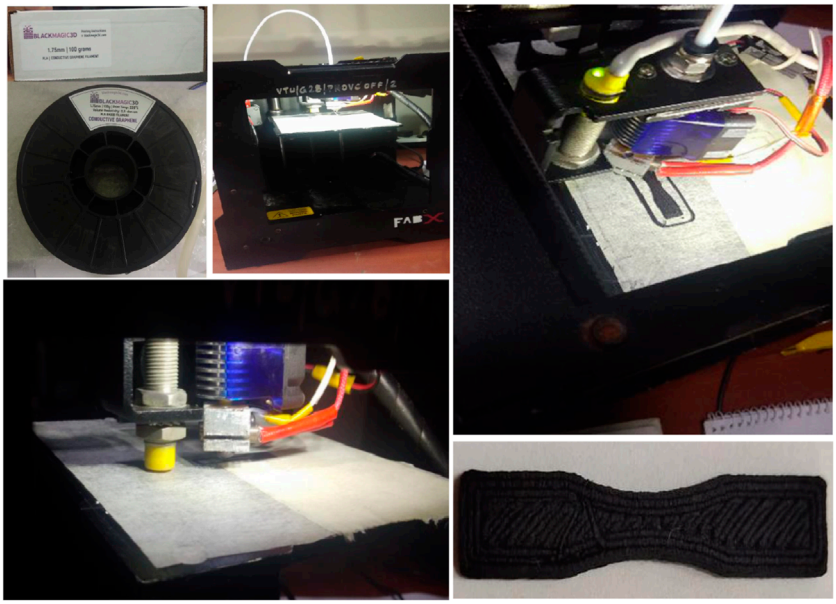

FIGURE 4
FDM printing process and printing model.

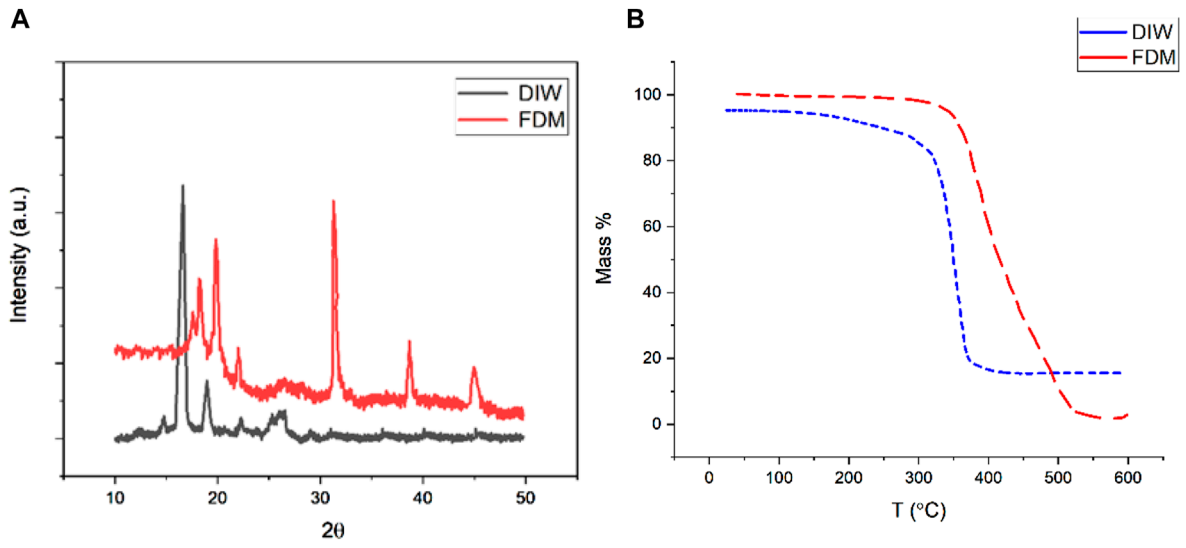

FIGURE 5
(A) "XRD pattern" and **(B)** "TGA analysis" for the variation for both DIW- and FDM-printed models.

PVA did not show any changes in the quick mass loss. FDM also showed the same level of reaction at the same temperature (280°C), but sudden changes were not observed like DIW. Due to the PLA content, the adjacent carbon atom did not lose the bond easily like DIW.

The viscosity of graphene for both printing methods (FDM and DIW) is considered the primary factor that leads to the good feasibility and quality of the printed model (Dervishi et al., 2019; Pinilla-Sánchez et al., 2022) (Figure 6A). A viscometer performed viscosity analyses for the FDM and DIW 3D-printed parts, ranging from 20°C to 35°C and 6 to 60 rpm for temperature and rotation speed, respectively. The thermostatic bath was used to regulate the surrounding temperature. The viscosity of DIW-based graphene was measured at temperatures of 25, 30, 35, 40, 45, 50, 55, and 65°C at regular intervals. FDM-based graphene's viscosity was measured at temperatures of 25, 27, 32, 37, 42, 47, 54, 57, and 64°C at regular intervals. At each peak value of temperature and specific concentration, three readings of value have been taken, which will measure the lower mark value and upper mark value of the capillary tube. Measurement values have been noted from

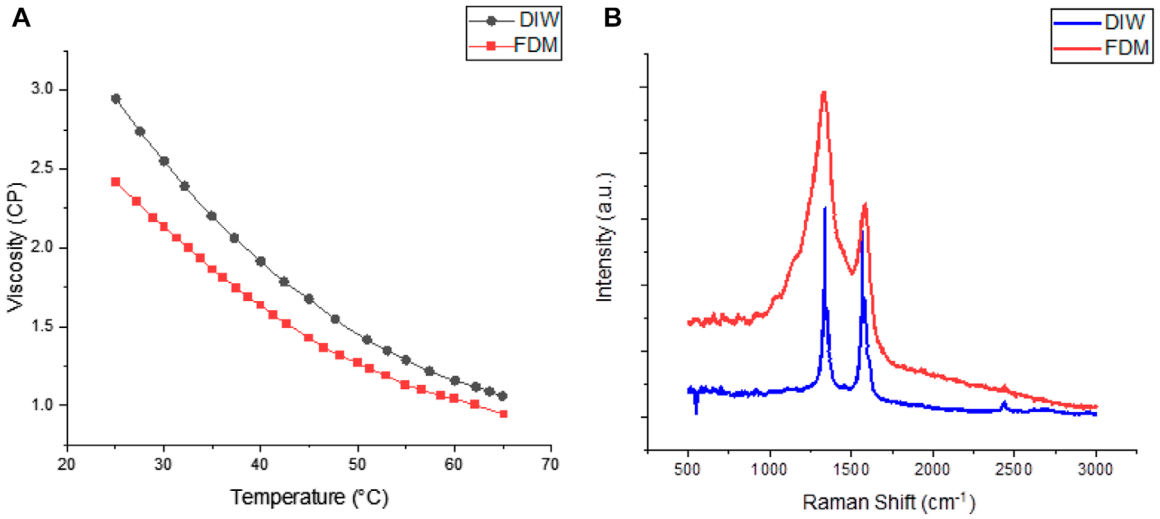

FIGURE 6
(A) "Viscosity analysis" and **(B)** "Raman shift analysis" for the variation for both DIW- and FDM-printed models.

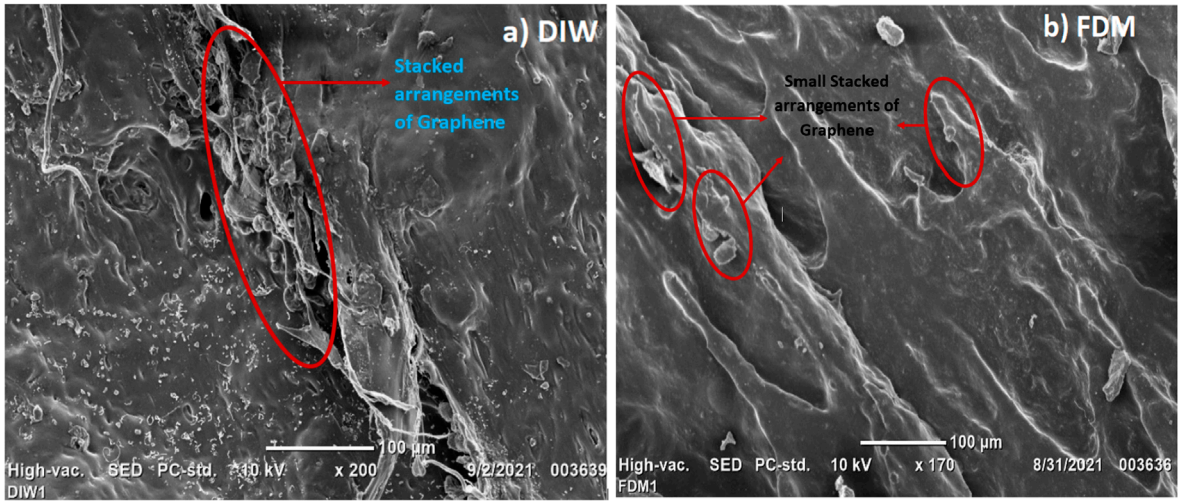

FIGURE 7
Scanning Electron Microscopy images of both **(A)** DIW- and **(B)** FDM-printed models.

the two sets of experiments, which will verify the results, and the final calculations have been formulated for an average of these two experiments. The different concentrations of the output printed model at various levels (0.15, 0.45, 0.65, 0.85, and 1.00%) were tested under various temperature conditions. The findings indicate that as the temperature increases, the viscosity consistently decreases.

Conversely, an increase in concentration leads to a rise in viscosity. In cases where the viscosity initially decreases, a subsequent stepwise increase is observed at certain temperature intervals. It is worth noting that the continuous increase in viscosity is directly proportional to the material concentrations. Both DIW and FDM exhibit similar levels of variation in viscosity with temperature. Raman spectroscopy has been considered one of the best tools to determine and differentiate the defective and defect-free areas for the output model (Lawal, 2019; Baghayeri et al., 2021). These Raman spectra characterized the prepared, printed output model. DIW- and FDM-printed models were tested for this analysis, as shown in Figure 6B. In both output models, this characterization allows the consideration of the conjugated area and carbon–carbon double bonds. This analysis allowed both the D-band and G-band to reach high-intensity peaks. The typical Raman spectrum of DIW-based graphene material is characterized by a G-band at 1,583.12 cm^{-1}, which matches with the E^2g phonon of the sp^2 of C atoms, and a D-band at 1,299.08 cm^{-1}, which matches with the living mode of k-point phonons of PVA symmetry. FDM-based graphene material is characterized by a G-band at 1,620.14 cm^{-1}, which is slightly shifted and varies from the position of the previous one. The D-band indicates down variation, which may change in the

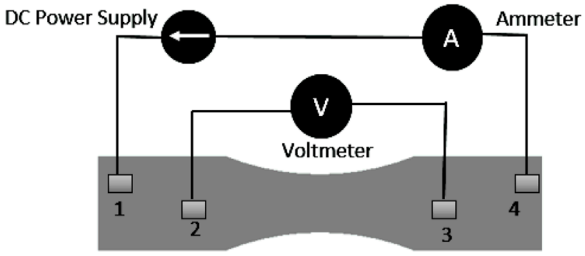

FIGURE 8
Four-point probe method connection setup.

rises from certain defective points and amorphous carbon species. The main intensity ratio of these two bands, which is indicated in the DIW- and FDM-based graphene output models, shows the quality of the product.

Scanning electron microscopy (SEM) is widely used for morphological method lysis of material characterization (Caminero et al., 2019; Choi et al., 2019). Due to heavy magnification conditions, Scanning Electron Microscopy has advantages like a large depth of focus and an ease of applicability. The resultant images (Figure 7) show the Scanning Electron Microscopy analysis of the printed graphene microstructure for both the FDM and DIW output models with the magnification ranges at 100 µm. In both the FDM- and DIW-printed models, the Scanning Electron Microscopy image data have shown variations in the morphology structure, A broad region with particle sizes specified at a magnification of 100 µm can be observed. As shown in both images, the distance between the graphene particles seems quite far, indicating that availability stacks are available in the printed graphene structure, which gives the graphene a layered structure. In the DIW Scanning Electron Microscopy image, the PLA particles appear smaller in size, and the collections are formed and equally spread over the entire surface area. It indicates that the stacked arrangements of the graphene layer act as a conductive pathway, which increases the graphene structure's conduction. The FDM Scanning Electron Microscopy image shows that the PVA with graphene has a rippled surface. The PVA particles in the graphene surface are smaller, and a uniform size of particles appears on the surface area. It clearly indicates a small stacked arrangement of the graphene layer. The combination of graphene material with PVA and PLA is responsible for the overall formation of the material structure in both FDM and DIW methods. The conductivity of DIW and FDM varies slightly due to the arrangement of stacked layers of graphene. Compared to PVA and PLA, the structure does not deviate from the graphene material. It is formed randomly from the graphene material in a thin layer tightly linked with other materials. Subsequently, it is formed from one layer to another in a regular solid surface structure. However, Scanning Electron Microscopy images reveal that the obtained graphene structure is not single-layered, indicating a reduction in the exfoliation structure of the graphene material. This reduction is evident in the smoother appearance of the built-up area on the surface. The four-point probe method is well-known for analyzing the material's electrical conductivity (Cultrera et al., 2019; Islam et al., 2019). The printed material was sequentially arranged in this procedure, and four distinct contacts were identified at equal intervals, as depicted in Figure 8. Copper wire has been utilized to establish connections with these four points. The process commences by altering the DC power supply from its initial value to the maximum value at regular intervals, specifically 2 V, 4 V, 6 V, and 8 V. As a result, significant fluctuations have been observed in both the voltage and ammeter readings.

Connection 2 is between points 1 and 4 and the DC power supply and ammeter. When the DC power supply has changed in regular intervals (2 V, 4 V, 6 V, and 8 V), notable changes have occurred in the ammeter and voltage, which are measured. Based on these variations in the voltmeter and ammeter, the

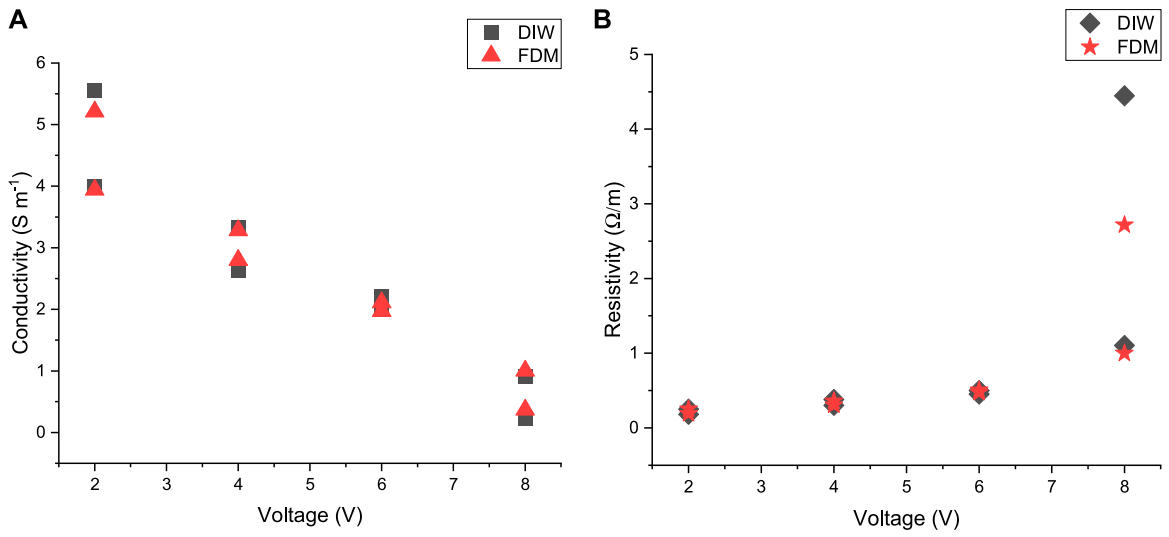

FIGURE 9
(A) Conductivity and **(B)** Resistivity (Ω/m) of the two printed models using FDM and DIW methods.

TABLE 3 Values for resistivity and conductivity.

S.No	Volt (V)	Resistivity (Ωm)		Conductivity (1/(Ωm)	
		DIW	FDM	DIW	FDM
1	2	5.56	5.21	0.17986	0.19194
2		4	3.94	0.25	0.25381
3	4	3.33	3.28	0.3003	0.30488
4		2.63	2.8	0.38023	0.35714
5	6	2.22	2.11	0.45045	0.47393
6		2	1.97	0.5	0.50761
7	8	0.906	1.00133	1.10375	0.99867
8		0.22486	0.3679	4.44727	2.71809

resistivity is calculated, and based on equation (1), the conductivity is calculated. This process is separately done for both DIW- and FDM-printed materials. Figures 9A, B show the material's resistivity and conductivity for both DIW- and FDM-printed materials. In both DIW- and FDM-printed models, the resistivity varies with the voltage in an increased manner. The same level of variation is shown in these graphs. It shows that both DIW and FDM have the same resistivity level. There is little difference between these two output graphs. Using equation (1), conductivity is calculated from the resistivity values, and based on the voltage input, it is calculated separately and mentioned in the ammeter and voltmeter. The same level of variations also appeared in conductivity. Both FDM and DIW show that once voltage started to increase, conductivity decreases, as mentioned in Table 3. From these changes derived from the above formula, we can calculate the value of resistivity and conductivity. The resistivity and conductivity for the two printed model have been calculated, and their results are shown in the same variations.

4 Conclusion

The present study examines the analysis of a graphene nanomaterial printed using two distinct 3D printing methods, namely, DIW and FDM. Two different analyses were conducted to evaluate these methods' impact on the printed models' electrical conductivity. Surprisingly, both 3D printed models exhibited similar variations in resistivity and conductivity. It is worth noting that the mechanical stability of the FDM- and DIW-based structures differed due to the presence of PLA and PVA content, respectively. However, this discrepancy did not affect the observed variations in conductivity and resistivity.

a) This research affirms that the presence of graphene at a concentration of 80% significantly influences conductivity calculation. Incorporating both PVA and PLA in the printing model contributes to the mechanical stability of the system independently.
b) This analysis has shown good results in the effect of printing parameters, such as building directions, infill rate percentage, infill patterns, print speed, extrusion temperatures, and layer height, independently on mechanical properties and dimensional accuracy.
c) The physical structure of the graphene nanomaterial remains unaffected and consistent, regardless of the printing methods employed. Therefore, it solely relies on the material's properties. Additionally, both the printed models are capable of maintaining their strength. Moreover, the density ratio does not exhibit a significant difference in the structure.

It is suggested that modifications be made to the combinations of the graphene composite with various materials, such as copper-based materials, derivatives of steel fibers, and layered transition metal oxides. These modifications are expected to enhance the electrical conductivity significantly.

Data availability statement

The original contributions presented in the study are included in the article/Supplementary Material; further inquiries can be directed to the corresponding author.

Author contributions

HR: conceptualization, data curation, formal analysis, funding acquisition, investigation, methodology, project administration, resources, writing–original draft, and writing–review and editing. MS: data curation, investigation, validation, visualization, and writing–review and editing. RC: conceptualization, methodology, project administration, resources, and writing–review and editing. SS: data curation, funding acquisition, investigation, project administration, and writing–review and editing. AM: formal analysis, methodology, project administration, resources, software,

and writing–review and editing. GS: conceptualization, formal analysis, funding acquisition, methodology, and writing–review and editing. HM: funding acquisition, investigation, methodology, project administration, and writing–review and editing. EA: funding acquisition, methodology, project administration, software, and writing–review and editing.

Funding

The author(s) declare financial support was received for the research, authorship, and/or publication of this article. This work was funded through the Researchers Supporting Project (RSP2024R164), King Saud University, Riyadh, Saudi Arabia.

Conflict of interest

The authors declare that the research was conducted in the absence of any commercial or financial relationships that could be construed as a potential conflict of interest.

Publisher's note

References

Adaris, M., Mayorga-martinez, C. C., and Pumera, M. (2020). 3D-printed graphene direct electron transfer enzyme biosensors. *Biosens. Bioelectron.* 151, 111980. doi:10.1016/j.bios.2019.111980

Agudosi, E. S., Abdullah, E. C., Numan, A., Mubarak, N. M., Khalid, M., and Omar, N. (2020). A review of the graphene synthesis routes and its applications in electrochemical energy storage. *Crit. Rev. Solid State Mater. Sci.* 45 (5), 339–377. doi:10.1080/10408436.2019.1632793

Arif, Z. U., Khalid, M. Y., Noroozi, R., Hossain, M., Shi, H. H., Tariq, A., et al. (2023a). Additive manufacturing of sustainable biomaterials for biomedical applications. *Asian J. Pharm. Sci.* 18, 100812. doi:10.1016/j.ajps.2023.100812

Arif, Z. U., Khalid, M. Y., Noroozi, R., Sadeghianmaryan, A., Jalalvand, M., and Hossain, M. (2022). Recent advances in 3D-printed polylactide and polycaprolactone-based biomaterials for tissue engineering applications. *Int. J. Biol. Macromol.* 218, 930–968. doi:10.1016/j.ijbiomac.2022.07.140

Arif, Z. U., Khalid, M. Y., Tariq, A., Hossain, M., and Umer, R. (2023b). 3D printing of stimuli-responsive hydrogel materials: literature review and emerging applications. *Giant* 17, 100209. doi:10.1016/j.giant.2023.100209

Baghayeri, M., Nabavi, S., Hasheminejad, E., and Ebrahimi, V. (2021). Introducing an electrochemical sensor based on two layers of Ag nanoparticles decorated graphene for rapid determination of methadone in human blood serum. *Top. Catal.* 65, 623–632. doi:10.1007/s11244-021-01483-4

Bikas, H., Stavropoulos, P., and Chryssolouris, G. (2016). Additive manufacturing methods and modelling approaches: a critical review. *Int. J. Adv. Manuf. Technol.* 83 (1–4), 389–405. doi:10.1007/s00170-015-7576-2

Caminero, M., Chacón, J., García-Plaza, E., Núñez, P., Reverte, J., and Becar, J. (2019). Additive manufacturing of PLA-based composites using fused filament fabrication: effect of graphene nanoplatelet reinforcement on mechanical properties, dimensional accuracy and texture. *Polym. (Basel)* 11, 799. doi:10.3390/polym11050799

Choi, S., Kim, C., Suh, J. M., and Jang, H. W. (2019). Reduced graphene oxide-based materials for electrochemical energy conversion reactions. *Carbon Energy* 1 (1), 85–108. doi:10.1002/cey2.13

Cultrera, A., Serazio, D., Zurutuza, A., Centeno, A., Txoperena, O., Etayo, D., et al. (2019). Mapping the conductivity of graphene with electrical resistance tomography. *Sci. Rep.* 9, 10655. doi:10.1038/s41598-019-46713-8

Daniel, N., and Liu, H. (2021). Comparative study on tribological behavior of graphene/polyimide and carbon fibers/polyimide composites: a review. *World J. Eng. Technol.* 09 (01), 26–50. doi:10.4236/wjet.2021.91003

Dervishi, E., Ji, Z., Htoon, H., Sykora, M., and Doorn, S. K. (2019). Raman spectroscopy of bottom-up synthesized graphene quantum dots: size and structure dependence. *Nanoscale* 11 (35), 16571–16581. doi:10.1039/c9nr05345j

Feng, Z., Li, Y., Xin, C., Tang, D., Xiong, W., and Zhang, H. (2019). Fabrication of graphene-reinforced nanocomposites with improved fracture toughness in net shape for complex 3D structures via digital light processing. *C* 5, 25. doi:10.3390/c5020025

Foster, C. W., Down, M. P., Zhang, Y., Ji, X., Rowley-Neale, S. J., Smith, G. C., et al. (2017). 3D printed graphene based energy storage devices. *Sci. Rep.* 7, 42233. doi:10.1038/srep42233

Gnanasekaran, K., Heijmans, T., van Bennekom, S., Woldhuis, H., Wijnia, S., de With, G., et al. (2017). 3D printing of CNT- and graphene-based conductive polymer nanocomposites by fused deposition modeling. *Appl. Mat. Today* 9, 21–28. doi:10.1016/j.apmt.2017.04.003

Guo, B., Liang, G., Yu, S., Wang, Y., Zhi, C., and Bai, J. (2021a). 3D printing of reduced graphene oxide aerogels for energy storage devices: a paradigm from materials and technologies to applications. *Energy Storage Mater.* 39, 146–165. doi:10.1016/j.ensm.2021.04.021

Guo, H., Zhao, H., Niu, H., Ren, Y., Fang, H., Fang, X., et al. (2021b). Highly thermally conductive 3D printed graphene filled polymer composites for scalable thermal management applications. *ACS Nano* 15, 6917–6928. doi:10.1021/acsnano.0c10768

Hou, Z., Lu, H., Li, Y., Yang, L., and Gao, Y. (2021). Direct ink writing of materials for electronics-related applications: a mini review. *Front. Mat.* 8, 1–8. doi:10.3389/fmats.2021.647229

Islam, M. R., Rahman, M., Farhad, S. F., and Podder, J. (2019). Structural, optical and photocatalysis properties of sol–gel deposited Al-doped ZnO thin films. *Surfaces Interfaces* 16, 120–126. doi:10.1016/j.surfin.2019.05.007

Ivanov, E., Kotsilkova, R., Xia, H., Chen, Y., Donato, R., Donato, K., et al. (2019). PLA/Graphene/MWCNT composites with improved electrical and thermal properties suitable for FDM 3D printing applications. *Appl. Sci. (Basel)* 9, 1209. doi:10.3390/app9061209

Jing, J., Chen, Y., Shi, S., Yang, L., and Lambin, P. (2020). Facile and scalable fabrication of highly thermal conductive polyethylene/graphene nanocomposites by combining solid-state shear milling and FDM 3D-printing aligning methods. *Chem. Eng. J.* 402, 126218. doi:10.1016/j.cej.2020.126218

Jo, G., Choe, M., Lee, S., Park, W., Kahng, Y. H., and Lee, T. (2012). The application of graphene as electrodes in electrical and optical devices. *Nanotechnology* 23, 112001. doi:10.1088/0957-4484/23/11/112001

Khalid, M. Y., Arif, Z. U., Noroozi, R., Hossain, M., Ramakrishna, S., and Umer, R. (2023a). 3D/4D printing of cellulose nanocrystals-based biomaterials: additives for sustainable applications. *Int. J. Biol. Macromol.* 251, 126287. doi:10.1016/j.ijbiomac.2023.126287

Khalid, M. Y., Kamal, A., Otabil, A., Mamoun, O., and Liao, K. (2023b). Graphene/epoxy nanocomposites for improved fracture toughness: a focused review on toughening mechanism. *Chem. Eng. J. Adv.* 16, 100537. doi:10.1016/j.ceja.2023.100537

Kristiawan, R. B., Imaduddin, F., Ariawan, D., Ubaidillah, H., and Arifin, Z. (2021). A review on the fused deposition modeling (FDM) 3D printing: filament processing, materials, and printing parameters. *Open Eng.* 11, 639–649. doi:10.1515/eng-2021-0063

Ku, M. J., Zhou, T. X., Li, Q., Shin, Y. J., Shi, J. K., Burch, C., et al. (2020). Imaging viscous flow of the Dirac fluid in graphene. *Nature* 583 (7817), 537–541. doi:10.1038/s41586-020-2507-2

Larraza, I., Vadillo, J., Calvo-Correas, T., Tejado, A., Olza, S., Peña-Rodríguez, C., et al. (2021). Cellulose and graphene based polyurethane nanocomposites for FDM 3D printing: filament properties and printability. *Polymers* 13, 839. doi:10.3390/polym13050839

Lawal, A. T. (2019). Graphene-based nano composites and their applications. A review. *A Rev. Biosens. Bioelectron.* 141, 111384. doi:10.1016/j.bios.2019.111384

Lei, L., Qiu, J., and Sakai, E. (2012). Preparing conductive poly (lactic acid) (PLA) with poly (methyl methacrylate) (PMMA) functionalized graphene (PFG) by admicellar polymerization. *Chem. Eng. J.* 209, 20–27. doi:10.1016/j.cej.2012.07.114

Liu, C., Huang, N., Xu, F., Tong, J., Chen, Z., Gui, X., et al. (2018). 3D printing technologies for flexible tactile sensors toward wearable electronics and electronic skin. *Polym. (Basel)* 10, 629. doi:10.3390/polym10060629

Liu, J., Ren, B., Lu, Y., Xi, X., Li, Y., Liu, K., et al. (2019). Novel design of elongated mullite reinforced highly porous alumina ceramics using carbonized rice husk as pore-forming agent. *Ceram. Int.* 45, 13964–13970. doi:10.1016/j.ceramint.2019.04.095

Mansour, M., Tsongas, K., and Tzetzis, D. (2019). Measurement of the mechanical and dynamic properties of 3D printed polylactic acid reinforced with graphene. *Polym. Technol. Mat.* 58 (11), 1234–1244. doi:10.1080/03602559.2018.1542730

Mattevi, S. C. (2021). Direct ink writing of energy materials As featured in. *Mater. Adv.* 2, 540–563. doi:10.1039/d0ma00753f

Mogan, J., Sandanamsamy, L., Halim, N. A., Harun, W. S., Kadirgama, K., and Ramasamy, D. (2021). A review of FDM and graphene-based polymer composite. *IOP Conf. Ser. Mater. Sci. Eng.* 1078, 012032. doi:10.1088/1757-899x/1078/1/012032

Ngo, T. D., Kashani, A., Imbalzano, G., Nguyen, K. T. Q., and Hui, D. (2018). Additive manufacturing (3D printing): a review of materials, methods, applications and challenges. *Compos. Part B* 143, 172–196. doi:10.1016/j.compositesb.2018.02.012

Noroozi, R., Arif, Z. U., Taghvaei, H., Khalid, M. Y., Sahbafar, H., Hadi, A., et al. (2023). 3D and 4D bioprinting technologies: a game changer for the biomedical sector? *Ann. Biomed. Eng.* 51, 1683–1712. doi:10.1007/s10439-023-03243-9

Papageorgiou, D. G., Kinloch, I. A., and Young, R. J. (2017). Mechanical properties of graphene and graphene-based nanocomposites. *Prog. Mater Sci.* 90, 75–127. doi:10.1016/j.pmatsci.2017.07.004

Pinilla-Sánchez, A., Chávez-Angel, E., Murcia-López, S., Carretero, N. M., Palardonio, S. M., Xiao, P., et al. (2022). Controlling the electrochemical hydrogen generation and storage in graphene oxide by *in-situ* Raman spectroscopy. *Carbon* 200, 227–235. doi:10.1016/j.carbon.2022.08.055

Rajpurohit, S. R., and Dave, H. K. (2019). Fused deposition modeling using graphene/PLA nano- composite filament. *Compos. Part A Appl. Sci. Manuf.* 85, 181–191. doi:10.1016/j.compositesa.2016.03.013

Sabet, M., and Soleimani, H. (2019). Inclusion of graphene on LDPE properties. *Heliyon* 5, e02053. doi:10.1016/j.heliyon.2019.e02053

Solís Pinargote, N. W., Smirnov, A., Peretyagin, N., Seleznev, A., and Peretyagin, P. (2020). Direct ink writing technology (3d printing) of graphene-based ceramic nanocomposites: a review. *Nanomaterials* 10 (7), 1300. doi:10.3390/nano10071300

Student-member, M. S., and Wolterink, G. (2020). A review of extrusion-based 3D printing for the fabrication of electro- and biomechanical sensors. *IEEE Sensors J.* 21, 12900–12912. doi:10.1109/JSEN.2020.3042436

Sun, Z., Fang, S., and Hu, Y. H. (2020). 3D graphene materials: from understanding to design and synthesis control. *Chem. Rev.* 120, 10336–10453. doi:10.1021/acs.chemrev.0c00083

Tarelho, J. P. G., Soares dos Santos, M. P., Ferreira, J. A. F., Ramos, A., Kopyl, S., Kim, S. O., et al. (2018). Graphene-based materials and structures for energy harvesting with fluids – a review. *Mat. TodayKidlingt.* 21, 1019–1041. doi:10.1016/j.mattod.2018.06.004

Tricot, F., Venet, C., Beneventi, D., Curtil, D., Chaussy, D., Vuong, T. P., et al. (2018). Fabrication of 3D conductive circuits: print quality evaluation of a direct ink writing process. *RSC Adv.* 8 (46), 26036–26046. doi:10.1039/c8ra03380c

Tsang, C. H., Huang, H., Xuan, J., Wang, H., and Leung, D. Y. (2020). Graphene materials in green energy applications: recent development and future perspective. *Renew. Sustain. Energy Rev.* 120, 109656. doi:10.1016/j.rser.2019.109656

Wei, X., Li, D., Jiang, W., Gu, Z., Wang, X., Zhang, Z., et al. (2015). 3D printable graphene composite. *Sci. Rep.* 5, 11181–11187. doi:10.1038/srep11181

Wincheski, B., Gardner, J., Sauti, G., Ruth, A., McVay, E., and Siochi, E. (2019). Direct printing of graphene sensors for health monitoring of additively manufactured structures. *AIP Conf. Proc.* 2102, 020007. doi:10.1063/1.5099711

Yang, L., Zeng, X., Ditta, A., Feng, B., Su, L., and Zhang, Y. (2020). Preliminary 3D printing of large inclined-shaped alumina ceramic parts by direct ink writing. *J. Adv. Ceram.* 9, 312–319. doi:10.1007/s40145-020-0369-6

Zhang, D., Chi, B., Li, B., Gao, Z., Du, Y., Guo, J., et al. (2016). Fabrication of highly conductive graphene flexible circuits by 3D printing. *Synth. Mater.* 217, 79–86. doi:10.1016/j.synthmet.2016.03.014